Inorg. Chem. **2007**, *46*, 1992–2001

Photophysical Properties of Highly Luminescent Copper(I) Halide Complexes Chelated with 1,2-Bis(diphenylphosphino)benzene

Akira Tsuboyama,*,† Katsuaki Kuge,† Manabu Furugori,† Shinjiro Okada,† Mikio Hoshino,‡ and Kazunori Ueno†

Leading-Edge Technology Development Headquarters, Canon Incorporated, Ohta-ku, Tokyo 146-8501, Japan, and The Institute of Physical and Chemical Research, Wako, Saitama 351-0198, Japan

Received May 11, 2006

Studies on synthesis, structures, and photophysics have been carried out for a series of luminescent copper(I) halide complexes with the chelating ligand, 1,2-bis[diphenylphosphino]benzene (dppb). The complexes studied are halogen-bridged dinuclear complexes, $[Cu(\mu\text{-}X)dppb]_2$ (X = I **(1)**, Br **(2)**, Cl **(3)**), and a mononuclear complex, $CuI(dppb)(PPh_3)$ **(4)**. These complexes in the solid state exhibit intense blue-green photoluminescence with microsecond lifetimes (emission peaks, λ_{max} = 492–533 nm; quantum yields, Φ = 0.6–0.8; and lifetimes, τ = 4.0–10.4 μs) at 298 K. In 2-methyltetrahydrofuran (2mTHF) solutions at 298 K, only **1** and **4** show weaker emission (Φ = 0.009) with shorter lifetimes (τ = 0.35 and 0.23 μs) and red-shifted spectra (λ_{max} = 543 and 546 nm). The emission in the solid state originates from the (M + X)LCT excited state with a distorted-tetrahedral conformation, in which emissive excited states, ^{1}(M + X)LCT and ^{3}(M + X)LCT, are in equilibrium with an energy difference of ~2 kcal/mol. On the other hand, the complexes in the 2mTHF solutions emit from the MLCT excited state with an energetically favorable flattened conformation in the temperature range of 298–130 K. The flattened geometry with equilibrated ^{1}MLCT and ^{3}MLCT states has a nonradiative rate at least 2 orders of magnitude larger than that of the distorted-tetrahedral geometry, leading to a much smaller emission quantum yield (Φ = 0.009) at 298 K. Since the flattening motion is markedly suppressed below 130 K, the emission observed in 2mTHF below 130 K is considered to occur principally from the (M + X)LCT state with a distorted-tetrahedral geometry. To interpret the photophysics of **1** and **4** in both the solid and solution states, we have proposed the "2-conformations with 2-spin-states model (2C × 2S model)". The electroluminescence device using **(1)** as a green emissive dopant showed a moderate EL efficiency; luminous efficiency = 10.4 cd/A, power efficiency = 4.2 lm/W at 93 cd/m^2, and maximum external quantum efficiency = 4.8%.

Introduction

Luminescent mono- and multinuclear copper(I) complexes have been extensively studied because they have possible applications in solar energy conversion, luminescence-based sensors, display devices, and probes of biological systems.[1−7] Among copper(I) complexes, the luminescence intensity of $[Cu(N{-}N)_2]^{1+}$, (N−N = 2,2′-bipyridine or 1,10-phenanthroline derivatives) markedly depends on the nature of the ligands.[5−9] For example, the copper(I) complex of phenanthroline, $[Cu(1,10\text{-phenanthroline})_2]^{1+}$, gives no luminescence in solutions. However, the complexes of 1,10-phenanthroline ligands with bulky substituents at the 2,9-positions exhibit luminescent behavior.

Systematic studies on the $[Cu(N{-}N)_2]^{1+}$ complexes carried out by McMillin and co-workers[5,8] have shown that lumi-

* To whom correspondence should be addressed. E-mail: tsuboyama.akira@canon.co.jp.

† Canon Inc.

‡ The Institute of Physical and Chemical Research.

(1) Bignozzi, C. A.; Argazzi, R.; Kleverlaan, C. J. *Chem. Soc. Rev.* **2000**, *29*, 87.

(2) Ford, P. C.; Cariati, E.; Bourassa, J. *Chem. Rev.* **1999**, *99*, 3625−3647.

(3) Balzani, V.; Campagna, S.; Denti, G.; Juris, A.; Serroni, S.; Venturi, M. *Acc. Chem. Res.* **1998**, *31*, 26.

(4) Roundhill, D. M. *Photochemistry and Photophysics of Metal Complexes*; Plenum Press: New York, 1994.

(5) McMillin, D. R.; McNett, K. M. *Chem. Rev.* **1998**, *98*, 1201−1219.

(6) Kutal, C. *Coord. Chem. Rev.* **1990**, *99*, 213−252.

(7) Ruthkosky, M.; Kelly, C. A.; Castellano, F. N.; Meyer, G. J. Coord. *Chem. Rev.* **1998**, *171*, 309−322.

10.1021/ic0608086 CCC: $37.00
Published on Web 02/27/2007

nescence originates from an MLCT (charge transfer from Cu to the ligand) excited state. The substituent effects of phenanthroline derivatives at 2,9-positions on the MLCT luminescence intensity have been explained by inhibiting the structural distortion from the tetrahedral to the flattened structure in the excited state. The major nonradiative process for the MLCT state is attributed to the structural distortion (flattening or rocking distortion). Thus, the introduction of the bulky substituents at the 2,9-positions of the phenanthroline ligands in $[Cu(N-N)_2]^{1+}$ effectively suppresses the extent of distortion in the MLCT state, leading to the high luminescence yields. The luminescence intensity and the emission peak energy of $[Cu(N-N)_2]^{1+}$ systems decrease with decreasing temperature. This result is explained well by the assumption that the ^{1}MLCT and ^{3}MLCT excited states are in thermal equilibrium. The energy separation between these two states is determined as 1800 cm^{-1}.[8a]

Miller et al. reported[9f] that a mixed ligand copper(I) complex with bulky substituents, $[Cu(dbp)(dmp)]^{1+}$ (dbp = 2,9-di-tert-butyl-1,10-phenanthroline, dmp = 2,9-dimethyl-1,10-phenanthroline), affords a significantly high luminescence quantum yield. Similarly, the mixed-ligand copper(I) complex with a sterically crowded diphosphine ligand, $[Cu(dmp)(POP)]^{1+}$ (POP = bis[2-(diphenylphosphino)phenyl]-ether), shows a high phosphorescence yield.[10] As is observed for these copper complexes, the bulky substituents of the ligand undergo effective suppression of the flattening distortion in the MLCT state.

Ford and co-workers[11] have reported that the tetranuclear copper(I) halide complexes $[CuXpy]_4$ (py = pyridine, X = halogen) and their derivatives show strong emission at room temperature in both the solid and solution states. The complexes exhibit visible photoluminescence emitting from two different excited states, one being a cluster-centered (^{3}CC) state and the other being a halogen-to-ligand charge transfer (^{3}XLCT) state. The emission from the ^{3}CC-excited-state is observable only for the complexes with a Cu···Cu distance shorter than the sum of the van der Waals radius (2.8 Å).

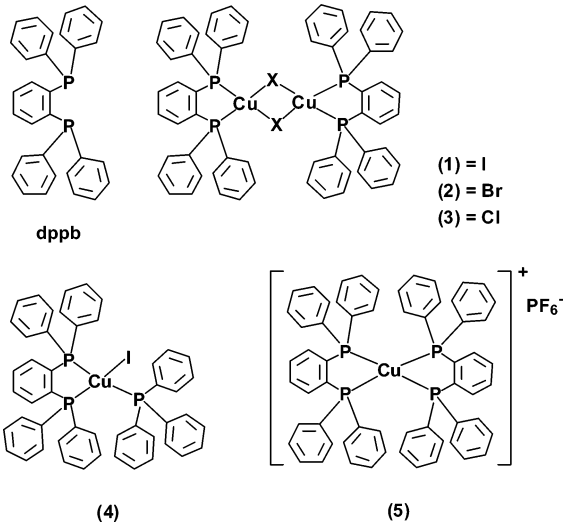

Figure 1. Copper complexes studied in this work.

Recently, Araki et al.[12] reported that halogen-bridged copper complexes, $[Cu_2(\mu\text{-}X)_2(PPh_3)L_n]$, with various heteroaromatic ligands (L) give intense emission at room temperature as well as at 80 K in the solid state. The long Cu···Cu distances (2.872−3.303 Å) observed in these complexes indicate no substantial interaction between the two copper(I) ions.

To date, a number of copper(I) complexes with phosphine ligands have been synthesized, and their emission properties are qualitatively discussed.[13] In the present paper, we study the emission of mono- and dinuclear copper complexes chelated with the bulky diphosphine ligand, 1,2-bis[diphenylphosphino]benzene (dppb). Figure 1 illustrates the molecular formulas of the copper(I) complexes studied. The photophysics of these complexes in both the solid and solution states are discussed on the basis of lifetime and quantum yield measurements in the temperature range of 77−298 K. An electroluminescence (EL) device fabricated

(8) (a) Kirchhoff, J. R.; Gamache, R. E.; Blaskie, M. W.; Del Paggio, A. A.; Lengel, R. K.; McMillin, D. R. *Inorg. Chem.* **1983**, *22*, 2380−2384. (b) Everly, R. M.; McMillin, D. R. *J. Phys. Chem.* **1991**, *95*, 9071−9075. (c) Everly, R. M.; Ziessel, R.; Suffert, J.; McMillin, D. R. *Inorg. Chem.* **1991**, *30*, 559−561. (d) Eggleston, M. K.; McMillin, D. R. *Inorg. Chem.* **1997**, *36*, 172−176. (e) Cunningham, C. T.; Cunningham, K. L. H.; Michalec, J. F.; McMillin, D. R. *Inorg. Chem.*, **1999**, *38*, 4388−4392. (f) Cunningham, C. T.; Moore, J. J.; Cunningham, K. L. H.; Fanwick, P. E.; McMillin, D. R. *Inorg. Chem.* **2000**, *39*, 3638−3644.

(9) (a) Sinozaki, K.; Kaizu, Y. *Bull. Chem. Soc. Jpn.* **1994**, *67*, 2435−2439. (b) Riesgo, E. C.; Hu, Y.; Bouvier, F.; Thummel, R. P.; Scaltrito, D. V.; Meyer, G. J. *Inorg. Chem.* **2001**, *40*, 3413−3422. (c) Schmittel, M.; Ganz, A.; Fenske, D.; Herderich, M. *J. Chem. Soc., Dalton Trans.* **2000**, 353−359. (d) Miller, M. T.; Gantzel, P. K.; Karpishin, T. B. *Inorg. Chem.* **1999**, *38*, 3414−3422. (e) Parker, W. L.; Crosby, G. A. *J. Phys. Chem.* **1989**, *93*, 5692−5696. (f) Miller, M. T.; Gantzel, P. K.; Karpishin, T. B. *J. Am. Chem. Soc.* **1999**, *121*, 4292−4293. (g) Kovalevsky, A. Y.; Gembicky, M.; Novozhilova, I. V.; Coppens, P. *Inorg. Chem.* **2003**, *42*, 8794−8802. (h) Chen, L. X.; Shaw, G. B.; Novozhilova, I.; Liu, T.; Jennings, G.; Attenkofer, K.; Meyer, G. J.; Coppen, P. *J. Am. Chem. Soc.* **2003**, *125*, 7022−7034. (i) Jahng, Y.; Hazelrigg, J.; Kimball, D.; Riesgo, E.; Wu, F.; Thummel, R. P. *Inorg. Chem.* **1997**, *36*, 5390−5395. (j) Felder, D.; Nierengarten, J.; Barigelletti, F.; Ventura, B.; Armaroli, N. *J. Am. Chem. Soc.* **2001**, *123*, 6291−6299.

(10) (a) Cuttell, D. G.; Kuang, S.; Fanwick, P. E.; McMillin, D. R.; Walton, R. A. *J. Am. Chem. Soc.* **2002**, *124*, 6−7. (b) Kuang, S.; Cuttell, D. G.; McMillin, D. R.; Fanwick, P. E.; Walton, R. A. *Inorg. Chem.* **2002**, *41*, 3313−3322.

(11) (a) Kyle, K. R.; Ryu, C. K.; DiBenedetto, J. A.; Ford, P. C. *J. Am. Chem. Soc.* **1991**, *113*, 2954−2965. (b) Kyle, K. R.; Ford, P. C. *J. Am. Chem. Soc.* **1989**, *111*, 5005−5006. (c) Ford, P. C. *Coord. Chem. Rev.* **1994**, *132*, 129−140.

(12) Araki, H.; Tsuge, K.; Sasaki, Y.; Ishizaka, S.; Kitamura, N. *Inorg. Chem.* 2005, *44*, 9667−9675.

(13) (a) Liaw, B.; Orchard, W.; Kutal, C. *Inorg. Chem.* **1988**, *27*, 1311−1316. (b) Aslanidis, P.; Cox, P. J.; Divanidis, S.; Tsipis, A. C. *Inorg. Chem.* 2002, *41*, 6875−6886. (c) Salem, G.; Schier, A.; Wild, B. *Inorg. Chem.* **1988**, *27*, 3029−3032. (d) Szlyk, E.; Kucharek, R.; Szymanska, I.; Pazderski, L. *Polyhedron*, **2003**, *22*, 3389−3393. (e) Black, J. R.; Levason, W.; Spicer, M. D.; Webster, M. *J. Chem. Soc., Dalton Trans.* **1993**, 3129−3136. (f) Bera, J. K.; Nethaji, M.; Samuelson, A. G. *Inorg. Chem.* **1999**, *38*, 218−228. (g) Xu, H.; Chen, Z.; Ishizaka, S.; Kitamura, N.; Wu, J. *Chem. Commun.* **2002**, 1934−1935. (h) Fournier, E.; Lebrun, F.; Drouin, M.; Decken, A.; Harvey, P. D. *Inorg. Chem.* **2004**, *43*, 3127−3135. (i) Harvey, P. D.; Drouin, M.; Zhang, T. *Inorg. Chem.* **1997**, *36*, 4998−5005. (j) Tsubomura, T.; Takahashi, N.; Saito, K.; Tsukuda, T. *Chem. Lett.* **2004**, *6*, 678−679. (k) Tsukuda, T.; Nakamura, A.; Arai, T.; Tsubomura, T. *Bull. Chem. Soc. Jpn.* **2006**, *79*, 288−290. (l) Kaltzoglou, A.; Cox, P. J.; Aslanidis, P. *Inorg. Chim. Acta* **2005**, *358*, 3048−3056. (m) Aslanidis, P.; Cox, P. J.; Divanidis, S.; Karagiannidis, P. *Inorg. Chim. Acta* **2005**, *357*, 1063−1076.

with the use of the dinuclear complexes **(1)** as an emissive dopant is also reported.

Experimental Section

Materials. Copper(I) iodide, copper(I) bromide, copper(I) chloride, triphenylphosphine, 1,2-bis(diphenylphosphino)benzene, and all solvents are commercially available (Aldrich) and were used as received.

Synthesis of Complexes. The dinuclear copper complexes **(1−3)** were prepared according to the following general procedure. A suspension of copper(I) halide (0.5 mmol) and 1,2-bis(diphenylphosphino)benzene (0.5 mmol, 223 mg) in 20 mL of toluene was stirred for 5 h at room temperature to form a pale-yellow precipitate. The precipitation was filtered off, washed with toluene, acetonitrile, and methanol, and then dried in vacuo. The yields of the precipitated complexes were 65% for **1**, 58% for **2**, and 60% for **3**. The pale-yellow powder was further purified by train sublimation with an argon stream under a pressure of 10^{-3} Torr at 330−360 °C to obtain pale-yellow block crystals of **1−3**.

The mononuclear complex **(4)** was prepared via the addition of triphenylphosphine to a suspension of complex **1** in 10 mL of toluene. The suspension was stirred for 3 h to form a clear and colorless solution. The solution was kept at room temperature; then the slow evaporation of the solvent gave white microcrystalline solids of **4**. The white solid was filtered off, washed with methanol, and dried in vacuo. Complex **5** was prepared according to the procedure from the previous paper.[13e]

[Cu(μI)dppb]$_2$ (1). Pale-yellow crystals. Yield after train sublimation: 48 mg, 15%. ^{1}H NMR($CDCl_3$, 298 K): δ 7.29−7.31 (m, 4H), 7.23−7.26 (m, 16H), 7.17−7.21 (m, 4H), 7.15 (t, 8H, J = 7.3 Hz), 7.04 (t, 16H, J = 7.3 Hz). ^{31}P NMR($CDCl_3$, 298 K): δ −22.1 (brs, $W_{1/2}$ = 176.1 Hz). Anal. Calcd for $C_{60}H_{48}Cu_2I_2P_4$: C, 56.57; H, 3.80. Found: C, 56.58; H, 3.80.

[Cu(μBr)dppb]$_2$ (2). Pale-yellow crystals. Yield after train sublimation: 53 mg, 18%. ^{1}H NMR ($CDCl_3$, 298 K): δ 7.27−7.30 (m, 20H), 7.18−7.20 (m, 4H), 7.15 (t, 8H, J = 7.5 Hz), 7.06 (t, 16H, J = 7.5 Hz). ^{31}P NMR ($CDCl_3$, 298 K): δ −19.0(s) (brs, $W_{1/2}$ = 224.7 Hz). Anal. Calcd for $C_{60}H_{48}Cu_2Br_2P_4$: C, 61.08; H, 4.10. Found: C, 61.20; H, 4.22.

[Cu(μCl)dppb]$_2$ (3). Yellow crystals. Yield after train sublimation: 44 mg, 16%. ^{1}H NMR ($CDCl_3$, 298 K): δ 7.27−7.30 (m, 20H), 7.19−7.21 (m, 4H), 7.16 (t, 8H, J = 7.5 Hz), 7.07 (t, 16H, J = 7.5 Hz). ^{31}P NMR ($CDCl_3$, 298 K): δ −17.2(s) (brs, $W_{1/2}$ = 214.2 Hz). Anal. Calcd for $C_{60}H_{48}Cu_2Cl_2P_4$: C, 66.06; H, 4.43. Found: C, 66.15; H, 4.42.

CuI(dppb)PPh$_3$ (4). White crystals (44 mg, 16%). ^{1}H NMR (THF-d_8, 230 K): δ 7.85−7.88 (m, 4H), 7.50−7.52 (m, 2H), 7.38−7.42 (m, 2H), 7.33 (t, 2H, J = 7.4 Hz), 7.23−7.29 (m, 7H), 7.17 (t, 6H, J = 7.4 Hz), 7.12 (t, 2H, J = 7.6 Hz), 7.07 (t, 6H, J = 6.9 Hz), 6.86 (t, 4H, J = 7.6 Hz), 6.60−6.64 (m, 4H). ^{31}P NMR ($CDCl_3$, 298 K): δ −10.0(s) (brs, $W_{1/2}$ = 191.9 Hz), 1.3(s) (brs, $W_{1/2}$ = 324.7 Hz) Anal. Calcd for $C_{48}H_{39}CuIP_3$: C, 64.11; H, 4.37. Found: C, 63.92; H, 4.53.

Measurement. Elemental analyses were carried out with an elemental analyzer Vario EL CHNOS from Elementar Co.

Photoluminescence spectra were recorded on a Hitachi F4500 fluorescence spectrometer. Spectral data were corrected with the use of a commercial standard light provided by Hitachi Co. Solid-state luminescence quantum yields (Φ) were determined with an organic electroluminescence spectrometer (Japan Optel Co.) equipped with an integrated sphere.[14] Luminescence quantum yields in solutions were determined with the use of an N_2-saturated toluene solution of 10^{-6} M *fac*-Ir(ppy)$_3$ (ppy = 2-phenylpyridine) as a reference (Φ[*fac*-Ir(ppy)$_3$] = 0.4).[15] Luminescence spectra at 77 K were measured in a 2-methyltetrahydrofuran (2mTHF). Emission lifetimes were measured by a Hamamatsu Photonics C4334 streakscope with excitation light (λ = 354.7 nm) from an Nd:YAG laser (Surelight-II from Continuum Co.). UV−vis spectra were recorded on a Shimadzu UV3100S spectrophotometer. Thermogravimetric and differential thermal analyses (TGA/DTA) were performed by a TG-DTA 2000S thermal analyzer (MAC Science Co.) under a N_2 stream with a scanning rate of 10 °C/min.

^{1}H NMR (500 MHz) and ^{31}P NMR (202 MHz) spectra were recorded on a Bruker AVANCE-500 NMR spectrometer.

X-ray Structure Analysis. Cubic crystals of **1−3** suitable for X-ray analysis were obtained with the train sublimation method in an argon stream. Needle crystals of **4** were obtained with a slow-diffusion method: we layered hexane (5 mL) onto a chloroform solution (5 mL) containing 10 mg of **4**. Diffraction data were collected at 93 K on a Rigaku RAXIS-RAPID imaging plate diffractometer equipped with graphite-monochromated Mo Kα radiation (λ = 0.71069 Å). Indexing was performed from 3 oscillations that were exposed for 90 (**1** and **3**) 30 **(2)**, and 60 **(4)** s. The crystal-to-detector distance was 127.40 mm. Readout was performed in the 0.100 mm pixel mode. The data were collected to a maximum 2θ value of 54.9°. A total of 73 **(1)**, 44 **(2)**, 83 **(3)**, and 55 **(4)** oscillation images were collected with two different goniometer settings. The exposure rates were 40.2 min for **1**, 10.2 min for **2**, and 30.0 min for **3** and **4** per deg. The crystal structures were solved with Patterson methods (DIRDIF99 PATTY) for **1** and **3** and direct methods (SIR92) for **2** and **4**. The crystal structures were refined by the full-matrix least-squares method on F^2. All non-hydrogen atoms were refined anisotropically, while hydrogen atoms were included but not refined. All analyses were performed by the crystallographic software package CrystalStructure. A summary of the refinement details and the resulting agreement factors is given in the Supporting Information (Table S1).

Electroluminescence Device. Electroluminescence (EL) devices were fabricated by the conventional vacuum deposition method.[16] The devices were made on an indium−tin oxide (ITO) film (15 Ω/cm^2, thickness 120 nm, from Nippon Sheet Glass Co.) with a 3.14 mm^2 round-patterned area. The organic materials for the EL devices were vacuum-deposited in turn on the ITO film at chamber pressures of less than 10^{-4} Pa, and aluminum was deposited over a KF layer as a cathode. The emissive layer was formed by codeposition of the emissive dopant, **1**, and the host molecule, 4,4′-*N*,*N*′-dicarbazolebiphenyl (CBP).

Results

1. X-ray Crystallographic Study. Major structural parameters of complexes **1−4** are summarized in Table 1. All the structural data are listed in the Supporting Information (Tables S3−S6). ORTEP plots of **1** and **4** are shown in Figure 2, and those of **2** and **3** are shown in the Supporting Information (Figure S1). The X-ray crystallographic studies on **1−3** reveal that two copper(I) centers are bridged by two halogen ligands to form a dinuclear structure with a four-membered Cu_2X_2 ring.

(14) de Mello, J. C.; Wittmann, H. F.; Friend, R. H. *Adv. Mater.* **1997**, *9*, 230−232.
(15) King, K. A.; Spellane, P. J.; Watts, R. J. *J. Am. Chem. Soc.* **1985**, *107*, 1431−1432.
(16) Tsuboyama, A.; Iwawaki, H.; Furugori, M.; Mukaide, T.; Kamatani, J.; Igawa, S.; Moriyama, T.; Miura, S.; Takiguchi, T.; Okada, S.; Hoshino, M.; Ueno, K. *J. Am. Chem. Soc.* **2003**, *125*, 12971−12979.

Table 1. Selected Structural Parameters for the Complexes **1**−**4**[a]

	1	**2**	**3**	**4**
	distances (Å)			
Cu−X	2.635	2.478	2.359	2.619
$Cu-P_{diphos}$	2.281	2.259	2.254	2.272
$Cu-P_{PPh3}$				2.249
Cu···Cu	2.898	2.837	2.866	
X···X	4.298	3.779	3.674	
	bond angles (deg)			
X−Cu−X	109.3	107.6	102.3	
Cu−X−Cu	66.7	69.8	74.8	
$P_{diphos}-Cu-P_{diphos}$	87.5	89.2	89.0	88.2
$P_{diphos}-Cu-P_{PPh3}$	-	-	-	123.0
	torsion angles (deg)			
$Cu-P_{diphos}-C-C$[b]	23.6	21.6	21.0	18.3
Cu−X−Cu−X	21.9	17.5	18.5	

[a] All parameters listed in the table are averaged. [b] Torsion angle around the P_{diphos}−C axis in a five-membered ring CuP_2C_2.

The copper(I) in the complexes **1**−**4** exhibits highly distorted tetrahedral coordination. In particular, the P−Cu−P angles ranging from 87.5 to 89.2° largely differ from the usual tetrahedral value because of the small bite angle of the dppb ligand. Although halogen-bridged copper complexes typically have a planar Cu_2X_2 geometry,[12,13b,17] the Cu_2X_2 rings of complexes **1**−**3** are significantly deformed by bending along the X···X axis.[13m] The dihedral angles between two CuX_2 triangles in Cu_2X_2 are 143.7, 124.5, and 150.9° for **1**, **2**, and **3**, respectively. As listed in Table 1, the Cu−X distances of **1**, **2**, and **3** elongate with an increase in the van der Waals radius of X, while their Cu···Cu distances are similar to each other (2.837−2.898 Å). The Cu···Cu distances are almost equal to the sum of van der Waals radius of copper (2.8 Å), indicating a minimum interaction between two copper atoms.

2. Photophysical Properties. (a) Absorption Spectrum. Figure 3 shows absorption spectra of **1**, **4**, **5**, and the free ligand, dppb, in 2mTHF solutions. These complexes have intense absorption bands (ϵ = 26 000−44 000 M^{-1} cm^{-1}) at ∼280 nm, which are assigned to the $\pi-\pi^*$ transition of the ligand, dppb. Mononuclear complex **5** contains two dppb ligands, and thus, the molar absorption coefficient of **5** at 280 nm is approximately two times larger than that of dppb.

The absorption spectra of the iodo complexes, **1** and **4**, exhibit broad shoulders (15 000 and 8000 M^{-1} cm^{-1}) at 330 nm and weak ones (4000 and 2000 M^{-1} cm^{-1}) at 380 nm. The absorption shoulders can be attributed to the electronic transition affected by the coppers, the iodide ligands, or both. As shown in Figure 4, Hartree−Fock calculations[18] carried out for **1** and **4** reveal that the electron density in the HOMO is distributed over the copper and iodine atoms, while that in the LUMO is localized on the ligands, dppb. Thus, the lowest excited states of **1** and **4** are a metal-to-ligand charge transfer (MLCT) state mixed with a halogen-to-ligand charge transfer (XLCT) state. The HOMO and LUMO calculations made for **5** indicated that the lowest excited state is attributed to the MLCT excited state.

(b) Emission Properties in the Solid State. Figure 5 shows the emission spectra of **1**−**3** in the solid state measured at 298 and 77 K. The spectra are broad without vibronic progressions, suggesting that the emissive excited states have the charge-transfer character. The λ_{max} values of dinuclear complexes **1**−**3** are in the order **1** < **2** < **3,** which is consistent with the order of ligand field strength of the halogen ions in the complexes ($I^- < Br^- < Cl^-$).[19] Obviously, the luminescent MLCT (π^*(dppb) ← d^{10}(Cu)) excited state is affected by the nature of the halogen ions directly bound to copper atoms. With a decrease in the ligand field strength, the energy separation of the d-orbitals decreases, leading to a larger MLCT (π^*(dppb) ← d^{10}(Cu)) energy and, therefore, to shorter λ_{max}. Taking the MO calculations into account, we consider that the emissive excited state of complexes **1**−**4** is attributed to the MLCT plus XLCT state, (M + X)LCT.

Complex **5**, which has no halogen ligand, was found to give an emission spectrum similar to those of complexes **1**−**4**. The emissive excited state of complex **5** is attributed to an MLCT excited state.

Part A in Figure 6 shows emission spectra of **1** measured at 77−300 K, obtained with an excitation wavelength of 350 nm in the solid state. Similar temperature-dependent emission spectra are observed for complex **4** (see Figure S2 in the Supporting Information). The time-resolved emission spectra are taken for complexes **1**−**4** with the 354.7 nm laser pulses. The spectra detected immediately after the laser pulse uniformly decay in the whole wavelength region observed. From the decay analysis in the temperature range of 77−300 K, the emission intensity is found to be expressed by a sum of the two exponential time functions

$$I = A_f \exp(-t/\tau_f) + A_s \exp(-t/\tau_s) \qquad [\tau_s > \tau_f] \qquad (1)$$

where τ_f and A_f are the lifetime and pre-exponential factor for the faster decay, respectively, and τ_s and A_s are those for the slower decay. The lifetimes, τ_f and τ_s, at 298 K are determined to be 1.5 and 4.0 μs for **1** and 4.0 and 8.5 μs for **4**. Since the time-resolved emission spectrum in the solid state is unchanged during the course of the whole decay, the faster and slower decay components are considered to have the same electronic nature: the emission in the solid state is assumed to occur from the two luminescence centers with different lifetimes. This assumption leads to the conclusion that the A factors, A_f and A_s, in eq 1 are proportional to the population of each luminescent center. The population ratio, γ_s, of the emissive state responsible for the slower decay is formulated as

$$\gamma_s = A_s/(A_s + A_f) \qquad (2)$$

(17) Henary, M.; Wootton, J. L.; Khan, S. I.; Zink, J. I. *Inorg. Chem.* **1997**, *36*, 796−801.

(18) Frisch, M. J.; Trucks, G. W.; Schlegel, H. B.; Scuseria, G. E.; Robb, M. A.; Cheeseman, J. R.; Zakrzewski, V. G.; Montgomery, J. A., Jr.; Stratmann, R. E.; Burant, J. C.; Dapprich, S.; Millam, J. M.; Daniels, A. D.; Kudin, K. N.; Strain, M. C.; Farkas, O.; Tomasi, J.; Barone, V.; Cossi, M.; Cammi, R.; Mennucci, B.; Pomelli, C.; Adamo, C.; Clifford, S.; Ochterski, J.; Petersson, G. A.; Ayala, P. Y.; Cui, Q.; Morokuma, K.; Malick, D. K.; Rabuck, A. D.; Raghavachari, K.; Foresman, J. B.; Cioslowski, J.; Ortiz, J. V.; Stefanov, B. B.; Liu, G.; Liashenko, A.; Piskorz, P.; Komaromi, I.; Gomperts, R.; Martin, R. L.; Fox, D. J.; Keith, T.; Al-Laham, M. A.; Peng, C. Y.; Nanayakkara, A.; Gonzalez, C.; Challacombe, M.; Gill, P. M. W.; Johnson, B. G.; Chen, W.; Wong, M. W.; Andres, J. L.; Head-Gordon, M.; Replogle, E. S.; Pople, J. A. *Gaussian 98*; Gaussian, Inc.: Pittsburgh, PA, 1998.

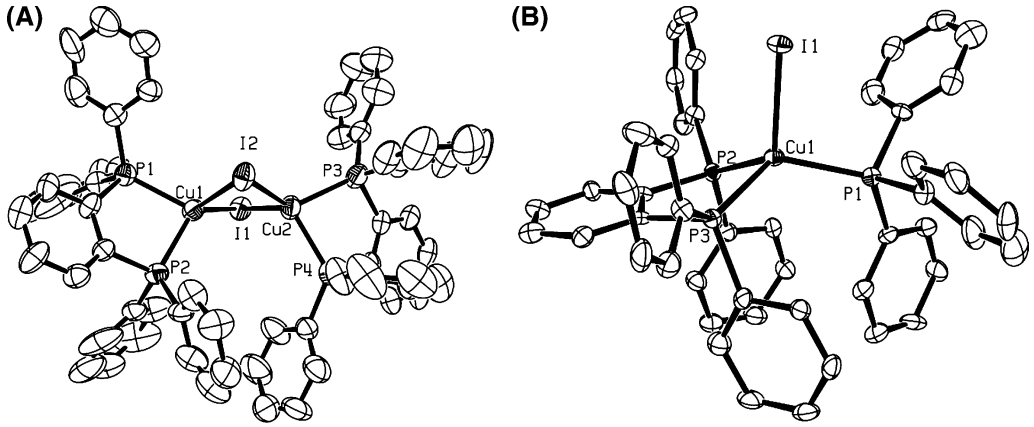

Figure 2. ORTEP diagrams of complexes (A) [Cu(μ-I)dppb]$_2$ **(1)** and (B) CuI(dppb)PPh$_3$ **(4)**.

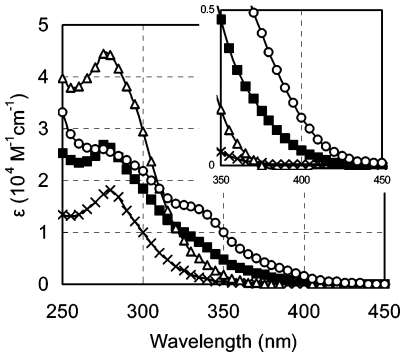

Figure 3. Absorption spectra of free ligand (×), complexes **1** (○), **4** (■), and **5** (△) in 2mTHF at 298 K. The inset shows a magnified view of the absorption edges.

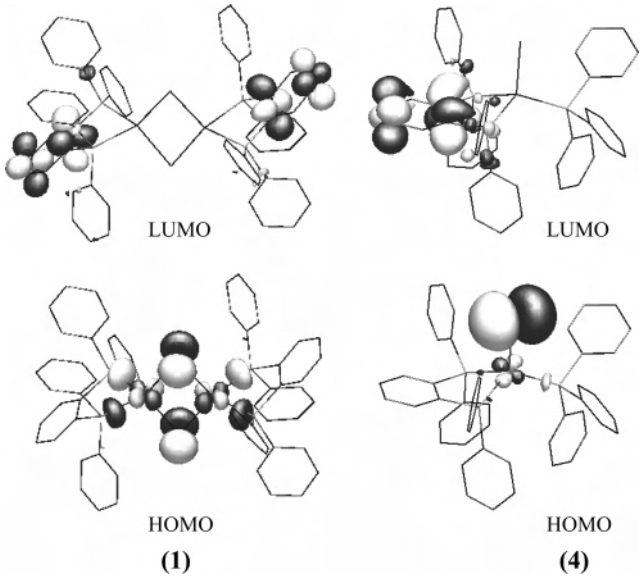

Figure 4. Molecular orbitals of complexes **1** and **4** calculated by the Hartree−Fock method using GAUSSIAN98.[18]

The value γ_s was found to be 0.67 for **1** and 0.35 for **4** in the range of 300−77 K. From eq 1, the ratio, R_s, of the emission yield for the slower decay component to that of the total yield is formulated as

$$R_s = A_s\tau_s/(A_f\tau_f + A_s\tau_s) \quad (3)$$

Since the values, R_s, of **1** and **4** are obtained as 0.88 and 0.60, respectively, in the temperature range of 300−77 K, the major luminescence from **1** and **4** is assigned to the slower decay component with the lifetime τ_s.

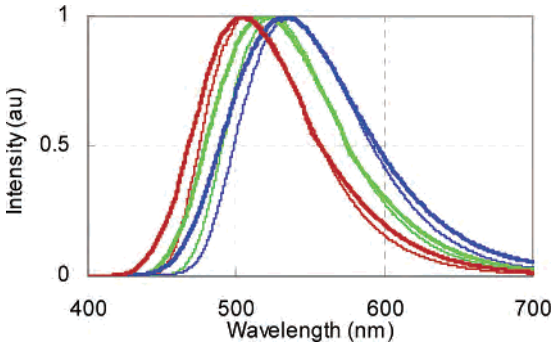

Figure 5. Normalized emission spectra of complexes **1**−**3** in the solid state at 298 K (thick line) and 77 K (thin line): red, **1**; green, **2**; blue, **3**.

The emission peaks, lifetimes, and emission yields of the copper complexes in the solid state at 77 and 298 K are summarized in Table 2. We found that (1) the lifetimes, τ, of luminescence from the solid states at 298 K are 2 or 3 orders of magnitude shorter than those at 77 K and (2) the total emission yield, Φ_T, decreases from 0.8 to 0.4 with a decrease in temperature from 298 to 77 K.

The emission yield, Φ, is generally formulated as

$$\Phi = \Phi_E k_r \tau \quad (4)$$

$$1 \geq \Phi_E \geq \Phi \quad (5)$$

Here, Φ_E, k_r, and τ denote the quantum yield for the formation of the emissive state, the radiative rate constant of the emissive state, and the observed emission lifetime, respectively. The emission yield of the slower component, Φ_s, is thus given by

$$\Phi_s = \Phi_T R_s = \Phi_E \gamma_s k_{r,s} \tau_s \quad (6)$$

where Φ_T, $k_{r,s}$, and τ_s denote the total emission yield, radiative rate constant, and lifetime of the slower component, respectively. Hereafter, we assume that $\Phi_E = 1.0$. With this assumption, γ_s, and τ_s in Table 2, the value of $k_{r,s}$ at 298 K is obtained as $\sim 2.6 \times 10^5$ s^{-1} for **1**. Similarly, the $k_{r,s}$ value

(19) Evans, D. R.; Reed, C. A. *J. Am. Chem. Soc.* **2000**, *122*, 4660−4667.

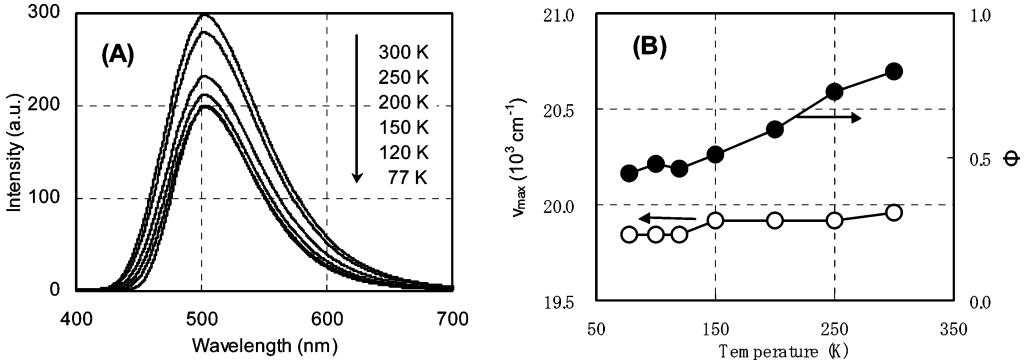

Figure 6. Temperature-dependent emission spectra of **1** in the range of 77−300 K in the solid state (A), and plots of the emission peak energy and quantum yield (Φ) vs temperature of **1** (B). Experimental errors in Φ are ±5%.

Table 2. Photophysical Parameters of **1**−**5** in the Solid State

	λ_{max} (nm)[a]		τ (μs)[b]		Φ[c]	
	298 K	77 K	298 K	77 K	298 K	77 K
free dppb		490		$>600 \times 10^3$		
1	502	505	4.0 (1.5)[d]	211 (50)[d]	0.8	0.44
2	520	524	4.3 (1.0)[d]	2300	0.6	
3	533	537	4.2 (2.5)[d]	2400	0.6	
4	492	503	8.5 (4.0)[d]	132 (66)[d]	0.8	0.41
5	495		10.4 (2.2)[d]			

[a] Emission peak wavelength. [b] Emission lifetime. Experimental errors are ±5%. [c] Emission quantum yield for the solid state. Experimental errors are ±5%. [d] Emission lifetime is composed of two components: $I = A_f \exp(-t/\tau_f) + A_s \exp(-t/\tau_s)$ [$\tau_s > \tau_f$, $A_s > A_f$]. The faster component, τ_f, is in parentheses.

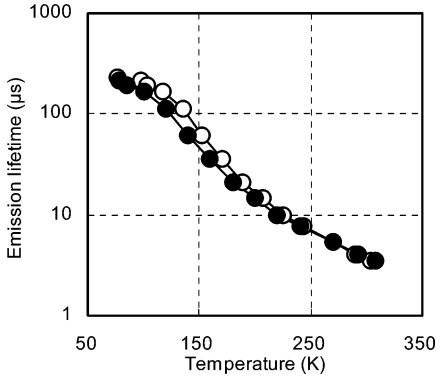

Figure 7. Temperature-dependent emission lifetimes, τ_s, of complexes **1** (○) and **4** (●) in the range of 77−300 K in the solid state. Experimental errors in τ_s are ±5%.

at 77 K is calculated to be $\sim 2.5 \times 10^3$ s^{-1}. The finding that $k_{r,s}$ at 298 K is 2 orders of magnitude larger than that at 77 K indicates that the emission at 298 K occurs from an electronic excited state different from that at 77 K.

The radiative rate constant, $k_{r,f}$, of the faster decay component of the emission from **1** was calculated to be 2.1×10^5 s^{-1} at 298 K and 3.1×10^3 s^{-1} at 77 K. These values are very close to those of the slower decay component. It, therefore, is concluded that the slower and faster decay components of the emission originate from the same electronic excited state. The difference in the lifetimes between the two components is probably attributable to the difference in the nonradiative decay processes.

Emission yields and lifetimes of **1** and **4** were measured in the temperature range of 77−300 K. Part B in Figure 6 displays the plots of the emission peak frequency (ν_{max}) and emission quantum yield (Φ) versus temperature for **1**. Similar plots for **4** are given in the Supporting Information (part B of Figure S2). The yields Φ gradually decrease on going from 300 to 77 K, and the ν_{max} values slightly shift to low frequency by 120 and 420 cm^{-1} for **1** and **4**, respectively. Figure 7 shows the temperature dependence of the emission lifetimes, τ_s, in the solid state for the complexes **1** and **4**. The usual expression of the emission lifetime is given by

$$\tau^{-1} = k_r + k_{nr} \tag{7}$$

where k_r and k_{nr} denote the radiative and nonradiative rate constant, respectively. When the emissive excited state is identical in the temperature range studied, the k_r value is inevitably independent of temperature. However, as described above, the k_r value at 298 K is ~2 orders of magnitude larger than that at 77 K. This indicates that the emissive state at 298 K differs from that at 77 K, and therefore, the lifetimes, τ, in the solid state cannot be described by eq 7. We, thus, assumed that two emissive states are in thermal equilibrium: a high-energy state with the rate constant k_H and a low-energy one with k_L. With the use of the equilibrium constant K, the lifetime τ is expressed as

$$\tau^{-1} = (k_L + k_H K)/(1 + K) \tag{8}$$

According to eq 8, the radiative rate constant of the complexes, τ_r^{-1} is represented as

$$\tau_r^{-1} = k_r = (k_{L,r} + k_{H,r} K)/(1 + K) \tag{9}$$

where $k_{L,r}$ and $k_{H,r}$ are the radiative rate constants of the low- and high-energy states, respectively. Since $K = A \exp(-\Delta H/RT)$, eq 9 is readily transformed to

$$\tau_r^{-1} = k_r = (k_{L,r} + k_{H,r} A \exp(-\Delta H/RT))/(1 + A \exp(-\Delta H/RT)) \tag{10}$$

Here ΔH is the enthalpy change between the high- and low-energy states.

For the slower decay component of the emission, eqs 9 and 10 are transformed to

$$\tau_{r,s}^{-1} = k_{r,s} = (k_{L,r,s} + k_{H,r,s} K_s)/(1 + K_s) = (k_{L,r,s} + k_{H,r,s} A_s \exp(-\Delta H_s/RT))/(1 + A_s \exp(-\Delta H_s/RT)) \tag{11}$$

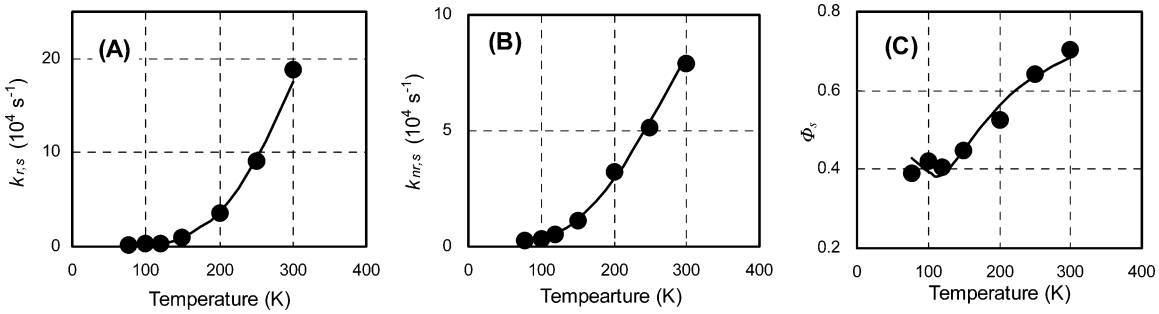

Figure 8. Radiative constant, $k_{r,s}$ (A), nonradiative constant, $k_{nr,s}$ (B), and emission quantum yield, Φ_s (C), for the slower decay component of **1** in the solid state, represented as a function of T. The solid lines were calculated with eqs 10−16 and the parameters listed in Table 3.

Table 3. Kinetic Parameters of the Slower Decay Component for **1** and **4** in the Solid State

	1	**4**
ΔH_s (kcal/mol)	1.9	2.3
$k_{L,r,s}$ (s^{-1})	2.0×10^3	2.1×10^3
$k_{H,r,s}$ (s^{-1})	1.0×10^8	1.0×10^8
A	0.041	0.042
ΔE_L (kcal/mol)	1.3	1.7
ΔE_H (kcal/mol)	0	0
$k_{L,nr,s}$ (s^{-1})	0.7×10^6	1.7×10^6
$k_{L,nr,s}(0)$ (s^{-1})	2.5×10^3	6.0×10^3
$k_{H,nr,s}$ (s^{-1})	0	0
$k_{H,nr,s}(0)$ (s^{-1})	0	0

Here, K_s is the equilibrium constant. The $\tau_{r,s}^{-1}$ ($= k_{r,s}$) values at various temperatures in eq 11 have been obtained from eq 6. Part A in Figure 8 shows the plot of $k_{r,s}$ versus T obtained for complex **1**. With the use of a weighted linear least-square fitting method, the parameters, $k_{L,r,s}$, $k_{H,r,s}$, ΔH_s, and a factor A_s in eq 11 are determined from the plot. The solid line in part A of Figure 8 is the calculated one with $k_{L,r,s} = 2.0 \times 10^3$ s^{-1}, $k_{H,r,s} = 1.0 \times 10^8$ s^{-1}, $\Delta H_s = 1.9$ kcal mol^{-1}, and $A_s = 0.041$ (see Table 3).

The temperature dependence of the emission yield is explained with the use of radiative and nonradiative rate constants which are expressed as a function of temperature. From eqs 7−9, the nonradiative rate constants, $k_{nr} = \tau_{nr}^{-1}$, of the complexes are given by

$$\tau_{nr}^{-1} = k_{nr} = (k_{L,nr} + k_{H,nr}K)/(1 + K) \qquad (12)$$

where $k_{L,nr}$ and $k_{H,nr}$ denote the nonradiative decay rate constants of the low- and high-energy states, respectively. For the slower decay component, $\tau_{nr,s}^{-1}$ is written as

$$\tau_{nr,s}^{-1} = (k_{L,nr,s} + k_{H,nr,s}K_s)/(1 + K_s) \qquad (13)$$

Because $t_s^{-1} = k_{r,s} + k_{nr,s}$, $t_{nr,s}^{-1}$ ($= k_{nr,s}$) is readily calculated by subtracting $k_{r,s}$ from τ_s^{-1}. Part B of Figure 8 shows the plot of $\tau_{nr,s}^{-1}$ ($= k_{nr,s}$) versus T obtained with complex **1**. The nonradiative rate constant k_{nr} is generally composed of the temperature-dependent and -independent terms. Thus, $k_{L,nr,s}$ and $k_{H,nr,s}$ are formulated as

$$k_{L,nr,s} = k_{L,nr,s}(0) + k_{L,nr,s}\exp(-\Delta E_L/RT) \qquad (14)$$

$$k_{H,nr,s} = k_{H,nr,s}(0) + k_{H,nr,s}\exp(-\Delta E_H/RT) \qquad (15)$$

respectively. We have made the least-squares calculation for $\tau_{nr,s}^{-1}$ according to eq 13. Table 3 lists the parameters $k_{L,nr,s}(0)$, $k_{L,nr,s}$, ΔE_L, $k_{H,nr,s}(0)$, $k_{H,nr,s}$, and ΔE_H obtained for complexes **1** and **4**. These values are found to reproduce well the plot of $\tau_{nr,s}^{-1}$ versus T as shown in part B of Figure 8 for **1** and in part B of Figure S3 for **4**.

Part C in Figure 8 shows the plots of emission quantum yields, Φ_s, of the slower decay component of the emission from **1**, represented as a function of T. The yield, Φ_s, for the slower component is written as

$$\Phi_s = \gamma_s k_{r,s}\tau_s = \gamma_s k_{r,s}/(k_{r,s} + k_{nr,s}) \qquad (16)$$

The plots of Φ_s versus T experimentally obtained fit well with the curve of Φ_s, which was calculated with eqs 12−16 and the parameters listed in Table 3.

Similar analytical procedures have been applied for the faster decay components of emission in the solid state (See Figure S4 and Table S2 in Supporting Information). The values ΔH, $k_{L,r,f}$, and $k_{H,r,f}$ obtained (listed in Table S2) are in good agreement with those of the corresponding slower decay components.

(c) Emission Properties in 2mTHF Solutions. Photoluminescence is observed only for **1** and **4** in a nitrogen-purged 2mTHF solution at 298 K. Similar luminescence spectra of **1** and **4** are observed for toluene and chloroform solutions. The emission spectra of complexes **1** and **4** in 2mTHF at 96−270 K are shown in part A of Figure 9 and in part A of Figure S5, respectively. Both **1** and **4** in fluid 2mTHF solutions at 270 K give emission spectra largely red-shifted by 45−57 nm in comparison with those in frozen glasses at 96 K. It is found that the emission quantum yields, Φ, of **1** at 298 K in solutions are very small (0.009) relative to those in the solid state (0.8).

The luminescence properties of dinuclear complex **1** and mononuclear complex **4** in the solutions are very similar to each other. It might be expected that the dinuclear complex **1** is produced from the mononuclear complex **4** according to the equilibrium reaction

$$2\ \mathrm{Cu(dppb)PPh_3}\ \textbf{(4)} \rightleftarrows [\mathrm{Cu}(\mu\text{-I})(\mathrm{dppb})]_2\ \textbf{(1)} + 2\mathrm{PPh_3} \qquad (17)$$

To examine whether **1** and **4** are in equilibrium or not, ^{31}P NMR studies of **1** and **4** were carried out. The ^{31}P NMR spectra are given in the Supporting Information (Figure S6). The ^{31}P NMR spectrum of **4** in a $CDCl_3$ solution was found to differ markedly from that of **1**, and no ^{31}P signal of free PPh_3 was observed. Therefore, the ^{31}P NMR analysis

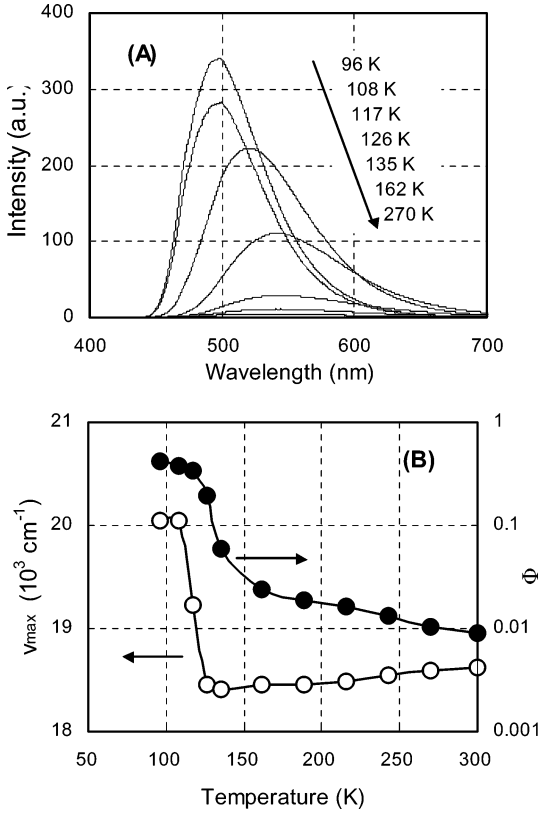

Figure 9. Emission spectra of **1** in the range of 96−300 K in 2mTHF solution (A) and plots of the emission peak energy (ν_{max}) and quantum yield (Φ) vs T for **1** (B). Experimental errors in Φ are ±5%.

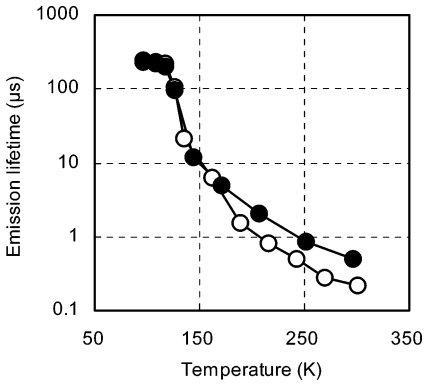

Figure 10. Temperature-dependent emission lifetimes of **1** (○) and **4** (●), respectively, in the range of 96−300 K in 2mTHF solutions. Experimental errors in τ are ±5%.

leads to the conclusion that complexes **1** and **4** are not in equilibrium.

Plots of ν_{max} and Φ versus T (part B of Figure 9 for **1** and part B of Figure S5 for **4**) represent a dramatic decrease in the emission intensity and a small low-frequency shift of ν_{max} with a decrease in temperature from 300 to 130 K. Below 130 K, a marked high-frequency shift of ν_{max} is observed in a narrow temperature range of 130−96 K. It is suggested that the emissive species in the range of 130−300 K differs from that below 130 K.

Figure 10 shows the temperature dependence of the emission lifetimes, τ, in 2mTHF solutions for **1** and **4**. The decay of emission in solutions follows first-order kinetics in the temperature range of 96−300 K. As mentioned above,

Table 4. Kinetic Parameters for the Decay of the Excited State of **1** and **4** in 2mTHF Solutions in the Temperature Range of 300−150 K

	1	**4**
ΔH (kcal/mol)	1.4	1.1
$k_{L,r}$ (s^{-1})	1.5×10^3	0.4×10^3
$k_{H,r}$ (s^{-1})	1.5×10^6	0.4×10^6
A	0.30	0.31
ΔE_L (kcal/mol)	3.0	4.5
ΔE_H (kcal/mol)	1.6	0.9
$k_{L,nr}$ (s^{-1})	2.1×10^8	1.0×10^8
$k_{L,nr}(0)$ (s^{-1})	0	0
$k_{H,nr}$ (s^{-1})	7.5×10^8	1.6×10^8
$k_{H,nr}(0)$ (s^{-1})	7.6×10^7	2.4×10^6

Table 5. Radiative Rate Constants for **1** and **4** in Frozen 2mTHF and the Solid State at 77 K

	solution (s^{-1})	solid (s^{-1})	
	2mTHF	slower decay	faster decay
1	$(1.4 \pm 0.2) \times 10^3$	$(2.5 \pm 0.4) \times 10^3$	$(3.1 \pm 0.4) \times 10^3$
4	$(1.4 \pm 0.2) \times 10^3$	$(5.3 \pm 0.4) \times 10^3$	$(3.8 \pm 0.4) \times 10^3$

the emission properties of **1** and **4** in the range of 300−130 K markedly differ from those in the range of 130−96 K. Thus, we deal with the kinetic analysis of the emission by dividing the temperature range into two regions: 300−130 and 130−96 K.

The lifetimes of emission from **1** and **4** in solution become long with a decrease in temperature in the range of 300−150 K. The radiative rate constants for **4** calculated from $k_r = \Phi/\tau$ are found to decrease from 1.8×10^4 to 4.8×10^3 s^{-1} with a decrease in temperature. The plot of k_r versus T is assumed to fit eq 9. By using a linear least-square fitting calculation, we determined the parameters $k_{L,r}$, $k_{H,r}$, A, and ΔH in 2mTHF solutions. In analogy with the case of the solid state, the kinetic parameters are also obtained for the nonradiative processes. The experimental values of k_r, k_{nr}, and Φ in 2mTHF fit well with the curve of those calculated with the use of eqs 10−16 (see Figure S7 in Supporting Information). As listed in Table 4, the kinetic parameters of the complexes in the present study are in moderate agreement with those of $[Cu(2,9\text{-dimethyl-}1,10\text{-phenanthroline})_2]^{1+}$ [ΔH = 5.1 kcal/mol, k_r(triplet) = 10^3 s^{-1}, k_r(singlet) = 10^7 s^{-1}].[8a]

Emission spectra of **1** and **4** in 2mTHF solutions below 130 K are similar to those observed for the solid state. The radiative rate constants in 2mTHF at 77 K are evaluated from $k_r = \Phi/\tau$. As listed in Table 5, the radiative rate constants of **1** and **4** in both the solid state and frozen solution at 77 K are ~10^3 s^{-1}.

3. EL Device. An EL device fabricated with **1** as a dopant in a multilayered structure is shown in part A of Figure 11. The layers in the device are composed of a hole-transporting layer (HTL), an emissive layer (EML), an electron-transporting layer (ETL), and an electron-injection layer (EIL). The materials used for the device are PF01 (4,4′-bis[phenyl(9,9′-dimethylfluorenyl)amino]biphenyl) for HTL (40 nm), **1** (10 wt %) in CBP (4,4′-*N*,*N*′-dicarbazolebiphenyl) for EML (20 nm), Bphen (4,7-biphenyl-1,10-phenanthroline) for ETL (50 nm), and KF for EIL (5 nm). The concentration of **1** in the EML was 10 wt %, which afforded the optimum external efficiency, η_{ex}. At concentrations of more than 10 wt %, η_{ex} tends to decrease because of self-quenching.

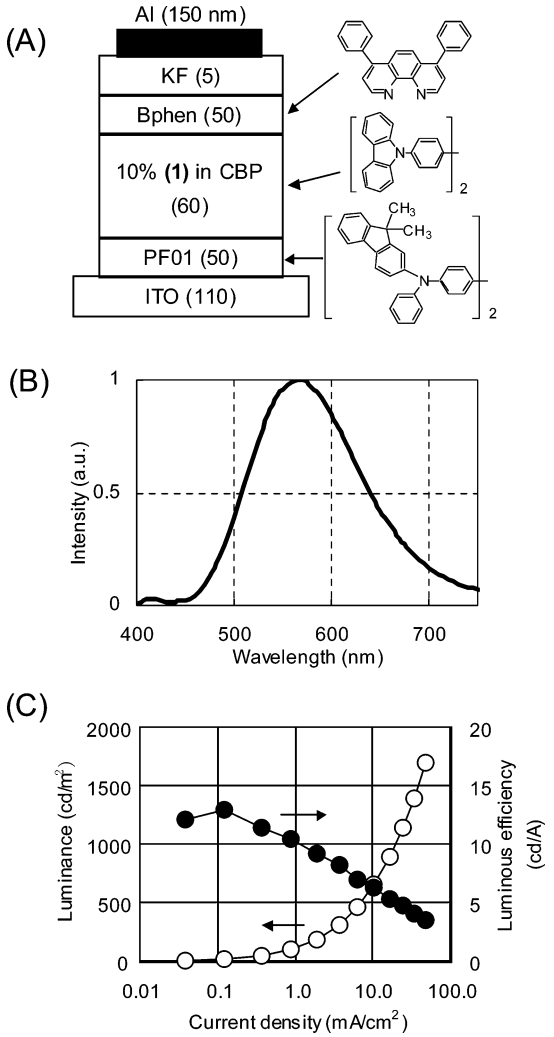

Figure 11. Electroluminescence (EL) device construction and molecular formulas of the compounds used in each layer (A), the EL spectrum (B), and plots of luminance and luminous efficiency vs current density of the EL device (C).

Parts B and C in Figure 11 display the EL spectrum and the plots of luminance and luminous efficiency versus current density, respectively. The maximum luminance obtained is 1700 cd/m^2 at 48 mA/cm^2. Luminous efficiency and power efficiency are moderate: 10.4 cd/A and 4.2 lm/W, respectively, at 93 cd/m^2. The maximum external efficiency of the device is 4.8% at 7 cd/m^2. The peak wavelength of the EL spectrum located at 565 nm significantly differs from that of photoluminescence (PL), 502 nm, in the solid state. The difference in the spectra between EL and PL will be discussed later. It is clear that the dinuclear complex (**1**) is useful as an emissive dopant in EL devices.

Discussion

(a) Emission in Solid State. Dinuclear complex **1** has emission spectra very similar to those of mononuclear complex **4**. As revealed by the X-ray structure analysis, the Cu···Cu distance of **1** is close to the sum of the van der Waals radii of two copper atoms. It is supposed that the interaction between the two copper atoms is very weak in both the ground and emissive excited states, and thus, the emission from **1** resembles that of complex **4**.

Complexes **1** and **4** in the solid state exhibit strong blue-green luminescence in the temperature range of 77−298 K. From the decay analysis, two luminescent centers in the solid state are found to give similar emission spectra with different lifetimes. On the basis of the fact that the radiative rate constants, k_r, of the emission from the two luminescent centers are in good agreement each other, the electronic states of the two centers are concluded to be identical.

The apparent k_r values at 298 K are found to be 2 orders of magnitude larger than those at 77 K. Thus, the emissive electronic state at 298 K is supposed to differ from that at 77 K. According to earlier studies,[5,8] we assumed that the two electronic states, high- and low-energy states, are in thermal equilibrium. From the lifetime analysis carried out for the slower decay component of the emission from **1** in the solid state, the radiative rate constant, $k_{H,r,s}$, for the higher-energy state is determined to be $k_{H,r,s} = 1.0 \times 10^8$ s^{-1}, which is 5 orders of magnitude larger than $k_{L,r,s}$ for the lower-energy state ($k_{L,r,s} = 2.0 \times 10^3$ s^{-1}). This result suggests that the higher- and lower-energy states are assigned to a spin-allowed ^{1}(M + X)LCT and a spin-forbidden ^{3}(M + X)LCT state, respectively. From the equilibrium constant, the energy separation, ΔH, between the two states is obtained as ∼2.0 kcal/mol for both complexes (**1** and **4**). The value of ΔH logically reflects the difference in energy, ΔE, between two states. We found that the ΔE value (1.2 kcal/mol) evaluated from the peak energy of emission spectra of **4** at 77 and 298 K is in moderate agreement with ΔH. However, the ΔE value of complex **1** (0.3 kcal/mol) is much smaller than ΔH. Presumably, the absorption edge of **1** at 298 K extends to wavelengths longer than that at 77 K, and thus, the emission spectrum measured at 298 K is shifted to red in appearance by the reabsorption of emission.

We observed that the quantum yields of emission from **1** and **4** in the solid state decrease with a decrease in temperature from 298 K to ∼140−150 K, and slightly increase below 140 K. This observation is explained as follows. For the slower decay component of emission from **1** in the solid state, emission at high-temperature principally occurs from ^{1}(M + X)LCT, which has $k_{H,nr} = 0$. At low temperatures, the emission process is principally governed by the lower-energy state, ^{3}(M + X)LCT, which has temperature-dependent $k_{L,nr}$. Thus, with a decrease in temperature, the contribution of the nonradiative processes from ^{3}(M + X)LCT becomes large, resulting in a decrease in the emission yield. Below 140 K, the nonradiative process of ^{3}(M + X)LCT is suppressed, and therefore, the emission yield begins to increase.

(b) Emission in 2mTHF. Copper complexes **1** and **4** in 2mTHF solutions show temperature-dependent emission spectra markedly different from those in the solid state. The spectra in 2mTHF below 110 K are similar to those observed for the solid state, probably because of the high viscosity of solvents: molecules **1** and **4** keep the tetrahedral form around the copper(I) atoms even in the excited state at low temperature. Therefore, we consider that the emission observed below 110 K originates from the (M + X)LCT state.

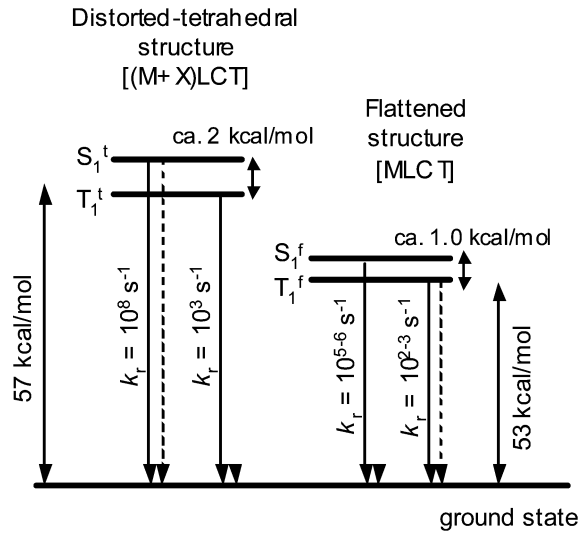

Figure 12. Schematic state diagram of the 2C × 2S model of the complexes.

A sharp red-shift of the emission band takes place, upon going from 110 to 130 K, within a narrow temperature range. Since the glass temperature of 2mTHF is ∼120 K, a dramatic decrease in viscosity may facilitate the conformation change from a tetrahedral to a flattened structure in the excited state, leading to the red shift of the emission band.

With an increase in temperature from 130 to 298 K, the spectra slightly shift to blue, and the emission yield decreases. The kinetic studies of emission from **1** and **4** in 2mTHF reveal that the temperature dependence of k_r in the range of 130−298 K is explained by the two spin-state models in the MLCT state: ^{1}MLCT and ^{3}MLCT are in thermal equilibrium. The ΔH values are determined to be 1.4 kcal/mol for **1** and 1.1 kcal/mol for **4**. Because ^{1}MLCT lies higher in energy than ^{3}MLCT, the emission spectrum shifts to blue with an increase in temperature. The difference in the peak energy of emission from **1** and **4** between 150 and 298 K was found to be almost identical to the ΔH value obtained. The emission lifetimes and quantum yields of the complexes in 2mTHF at 298 K are ∼1 order of magnitude smaller than those in the solid state, indicating that the MLCT excited state of the flattened conformation has nonradiative rate constants much larger than those of the tetrahedral one.

On the basis of the emission studies of the copper(I) complexes in 2mTHF solutions in the temperature range from 77 to 298 K, the complexes are concluded to take two conformations in the excited state: distorted tetrahedral and flattened geometry. Each conformation has two spin states, singlet and triplet states. Figure 12 shows a proposed schematic diagram of the "2-conformations with 2-spin-states model (2C × 2S model)" of the copper complexes mentioned above.

(c) EL Device. The dinuclear complexes are thermally stable and exhibit strong luminescence at room temperature. Consequently, the copper complexes studied in the paper are promising candidates for emissive materials of EL devices. The emission peak of EL (565 nm) originating from complex **1** is found at wavelength longer than that of photoluminescence (502 nm) in the solid state. Further, the emission spectrum from the EL device is very similar to that observed for the 2mTHF solution of the complex **(1)** at ∼140 K. This result suggests that the emissive state in the EL device has a conformation close to the flattened structure. Copper complex **1** in the device is superimposed on an amorphous host layer of CBP. Since the viscosity governs the conformation of the MLCT excited state, it is likely that the microscopic viscosity of CBP around complex **1** at 298 K is roughly equivalent to that of 2mTHF at ∼140 K.

Supporting Information Available: ORTEP diagrams, the temperature-dependent emission spectra, results of kinetic parameter analysis, ^{31}P NMR charts, TGA/DTA curves, and a summary of the refinement details, the resulting agreement factor, and all structural parameters of complexes **1**−**4**. This material is available free of charge via the Internet at http://pubs.acs.org.

IC0608086